

Appendix of RaUF

Anonymous CVPR submission

Beyond the F-score and CPR results summarized in Tab. 2 in the paper, this Appendix presents additional evaluations, including CD, F-score, and CPR, to offer a more complete performance results about the ablation study in Sec. 1 and 2. In addition, to validate the proposed method’s capability in generalization and its strength in handling ill-posed geometric inference arising from ambiguous feature-to-label mappings, we provide additional intuitive Bird’s-Eye View visualizations comparing different methods across various scenarios in Sec. 3 of the Appendix.

1. Performance on RaDelft Dataset

Detection Methods	Scene 1			Scene 2			Scene 4			Mean		
	CD (m) ↓	F-score ↑	CPR ↓	CD (m) ↓	F-score ↑	CPR ↓	CD (m) ↓	F-score ↑	CPR ↓	CD (m) ↓	F-score ↑	CPR ↓
Ours (w.o. NLL)	7.96	0.20	0.82	2.62	0.52	0.46	6.34	0.30	0.57	5.64	0.34	0.62
Ours (w.o. BDA)	5.98	0.27	0.76	2.00	0.60	0.39	3.43	0.47	0.58	3.80	0.45	0.57
Ours (w.o. GS)	3.84	0.36	0.70	1.32	0.70	0.39	1.82	0.53	0.54	2.32	0.53	0.54
Ours	3.79	0.36	0.72	1.30	0.69	0.41	1.74	0.54	0.50	2.27	0.53	0.54

Table 1. Comparison of spatial detection performance across different scenes and ablation configurations on the RaDelft dataset.

2. Performance on Self-Collected Dataset

Detection Methods	Sequence 1			Sequence 2			Sequence 3			Mean		
	CD (m) ↓	F-score ↑	CPR ↓	CD (m) ↓	F-score ↑	CPR ↓	CD (m) ↓	F-score ↑	CPR ↓	CD (m) ↓	F-score ↑	CPR ↓
Ours (w.o. NLL)	1.17	0.42	0.67	0.88	0.50	0.62	2.72	0.21	0.85	1.59	0.37	0.71
Ours (w.o. BDA)	0.94	0.56	0.55	0.42	0.73	0.38	1.63	0.31	0.79	0.99	0.53	0.57
Ours (w.o. GS)	0.85	0.60	0.48	0.42	0.74	0.39	1.61	0.32	0.78	0.96	0.55	0.55
Ours	0.80	0.58	0.54	0.35	0.81	0.27	1.53	0.39	0.71	0.89	0.59	0.50

Table 2. Comparison of spatial detection performance across different scenes and ablation configurations on the Self-Collected dataset.

The uncertainty-free variant (**Ours** (w.o. NLL)) exhibits worse effectiveness (CD ↑ about 2×) and reduced reliability (CPR ↑ about 15~40%) relative to the full model. This demonstrates that our uncertainty-learning strategy effectively alleviates ill-posed geometric inference arising from ambiguous feature-to-label mappings, thereby improving the model’s generalization capability.

In addition, removing the BDA module leads to decreases of 11~67% in effectiveness and 12% in reliability, indicating that BDA effectively exploits the mutual complementarity between spatial structure and Doppler coherence, thus enhancing feature robustness under cluttered conditions.

Moreover, our method supports Gaussian Sampling (GS). After sampling from the estimated uncertainty ellipsoids, the performance shows an improvement of 6% in F-score and a reduction of about 7% in CD, confirming that sampling from our anisotropic uncertainty distribution can enhance point-cloud quality and density while preserving reliability. This capability not only provides calibrated confidence estimates, but also establishes a new paradigm for point-cloud enhancement through adaptive, scale-aware Gaussian sampling tailored to the underlying uncertainty structure.

022 3. Bird's-Eye View Visualization

023 To visually illustrate the anisotropic uncertainty distribution of radar measurements, we downsample the point set together with the associated uncertainty ellipsoids to 200 instances for clearer presentation, as shown Fig 1.

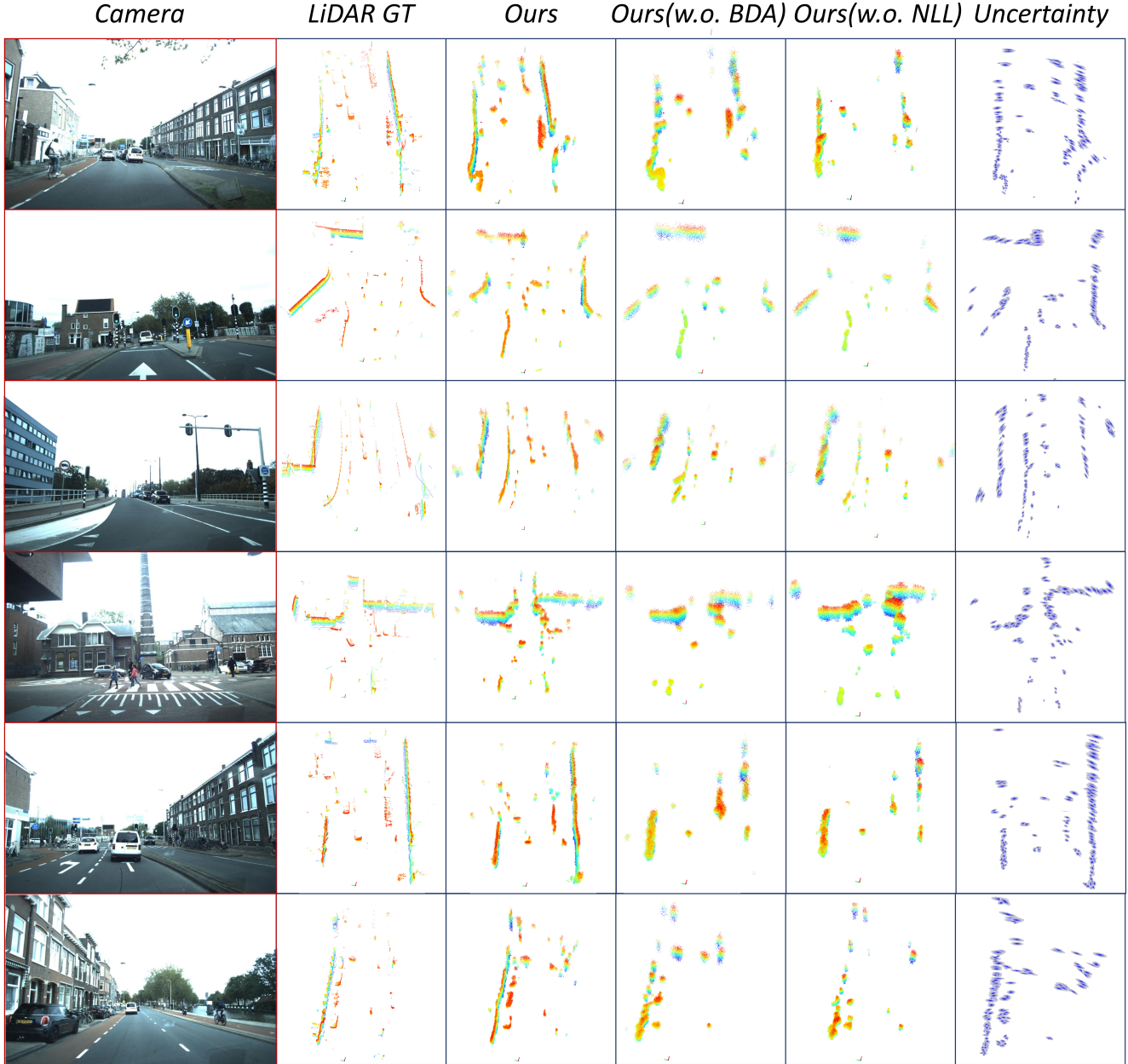


Figure 1. Bird's-Eye View visualization of Radar point clouds augmented by various methods and LiDAR ground truth.

024 From Fig. 1, our method produces denser and more structurally faithful point clouds than various ablation configurations,
 025 highlighting its strong capability in resolving geometric ambiguities induced by unreliable feature-label associations. Each
 026 ellipsoid is parameterized by the eigenvalues of the predicted covariance, where the length of the i -th principal axis is given
 027 by $a_i = 4\sqrt{\lambda_i \sqrt{\chi_2^2(p)}}$, with λ_i denoting the corresponding eigenvalue and $\chi_2^2(p)$ the Chi-square quantile at confidence level
 028 $p=90\%$. This construction ensures the ellipsoids clearly reflect the directional uncertainty encoded in the covariance structure.
 029